LAWRENCE LIVERMORE NATIONAL LABORATORY

UCRL-JC-155216

2ω Laser Propagation and Raman Backscatter in Underdense Gasbag Plasmas

N. B. Meezan, L. Divol, L. J. Suter, and M. C. Miller, LLNL

R. M. Stevenson, G. E. Slark, and K. Oades, AWE Aldermaston

September 5, 2003

This article was submitted to the Third International Conference on Inertial Fusion Sciences and Applications, Monterey, CA, September 7-12, 2003.

Auspices Statement

This work was performed under the auspices of the U.S. Department of Energy by University of California, Lawrence Livermore National Laboratory under Contract W-7405-Eng-48.

FPo5.46

2ω LASER PROPAGATION AND RAMAN BACKSCATTER IN UNDERDENSE GASBAG PLASMAS

N. B. Meezan, L. Divol, L. J. Suter, and M. C. Miller

Lawrence Livermore National Laboratory, P.O. Box 808, Livermore, CA, 94551-0808, meezan1@llnl.gov

R. M. Stevenson, G. E. Slark, and K. Oades

Atomic Weapons Establishment, plc., Aldermaston, Berkshire, U.K.

ABSTRACT—*Recent 2ω gasbag experiments on the Helen laser studied single-beam propagation and backscatter as a function of gas density. We present a comprehensive analysis of these experiments using simulations in HYDRA. Post-processed results agree well with experimental fast x-ray images (FXI) showing stable laser propagation across the bag. The measured total stimulated Raman backscatter (SRS) increases with initial gas density up to $n_e \approx 0.08\ n_c$, then decreases. Near-backscatter images (NBI) show that the decrease in total SRS with increasing density is not due to scatter outside of the collection optics. SRS gain spectra calculated from the HYDRA results agree well with experimental streak spectra. The tilt and spread in wavelength of the spectra appear to be explained by gasbag hydrodynamics only, with no need to invoke filamentation. Axial density gradients and laser pump absorption may combine to detune and limit SRS gain at high density.*

I. INTRODUCTION

The prospect of operating the National Ignition Facility (NIF) at 2ω offers several potential advantages to reaching ignition. Capsule designs that take advantage of high absorbed power and large fuel mass can obtain robust, high-yield burns. Unfortunately, high $I\omega^2$ and long length-scales can lead to destructive parametric instabilities. Filamentation and stimulated Raman (SRS) and Brillouin (SBS) backscatter can degrade hohlraum conversion efficiency and symmetry control. Hot electrons generated by SRS saturation can catastrophically pre-heat the capsule fuel. Surmounting these problems requires a solid understanding of 2ω laser propagation and backscatter in long, underdense plasmas.

II. GASBAG EXPERIMENTS AT HELEN

Four sets of experiments have been conducted at AWE's Helen laser to investigate 2ω propagation and interaction physics. Gasbag targets were used to approximate the long, underdense plasmas that would occur in a NIF 2ω ignition hohlraum. An LLNL gasbag consists of an aluminum washer of inner diameter 2.8 mm and thickness 0.4 mm with a thin plastic (polyimide) skin bonded to each end. A gasbag forms an oblate ellipsoid ≈2.4 mm long when inflated to 1 atmosphere, with a skin thickness of 350-400 nm[1]. The gasbags were filled with neopentane (C_5H_{12}) to obtain SRS-producing plasmas with electron densities 4% to 26% of the critical density.

One arm of the Helen laser was used to generate a 1 ns square pulse with 300-400 J of energy. The shots described here used a phase zone plate[2] (PZP) to focus the beam to a smooth, flat (4^{th}-order super-Gaussian) 250 μm diameter spot on the surface of the front skin, corresponding to an average intensity $I \approx 8 \times 10^{14}$ W/cm^2. The optical train had an overall f-number of about 3. Unlike previous gasbag experiments performed at multi-beam facilities[3], these experiments do not propagate an interaction beam through a pre-formed plasma. Laser propagation and interaction occur simultaneously.

A schematic of the experimental setup used at Helen is shown in Fig. 1. A side-on fast x-ray imaging camera (FXI) imaged the bags to observe propagation and hydrodynamics. A 25 μm thick beryllium filter shielded x-rays below about 1 keV. A small amount (1 % partial pressure) of krypton was added to some bags to enhance the x-ray images. The SRS station collected light

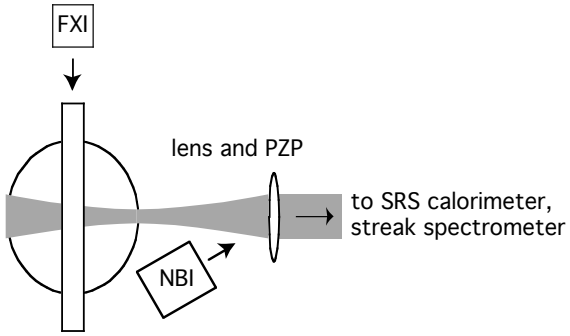

Fig. 1. Schematic of Helen gasbag experiments.

scattered back into the main focusing optics. A calorimeter measured total (time-integrated) backscatter, while a streak camera and grating spectrometer recorded time-resolved spectra. To give a qualitative estimate of the SRS scattered outside the collection optics, a filtered near-backscatter imaging (NBI) camera was focused on a diffuse aluminum plate surrounding the beam entrance window. A similar set-up was used to measure SBS.

III. SIMULATIONS AND MODELING

III.A. Hydrodynamics simulations in HYDRA

Radiation-hydrodynamics simulations of the gasbags were performed in HYDRA to assist in the analysis of the experiments. HYDRA is a multi-physics code developed by M. M. Marinak at LLNL for ICF simulations[4]. The gasbags were modeled in 2-D as 2.4 mm diameter hemispherical wedges. HYDRA's laser ray-tracing package models inverse bremsstrahlung absorption and includes bulk refraction, ponderomotive effects, and turning-point energy deposition, but does not simulate small-scale laser-plasma physics. The simulations used 600 rays. The actual (experimental) shot energy was used for each simulation.

HYDRA models flux-limited electron thermal conduction. The flux limiter was set to 1 for these simulations, i.e., the maximum heat flux allowed across a given surface was the one-way energy flux for a Maxwellian about the local electron temperature. The simulations also included multigroup radiation diffusion with tabular LTE opacities. The opacities were used primarily for post-processing (radiation transport is not very important for these low-Z plasmas). The hydrodynamics for these simulations were fully Lagrangian. The quotidian equation of state[5] (QEOS) with separate electron and ion temperatures was used for all materials. The aluminum washer was not modeled.

III.B. Synthetic FXI images

The results of each HYDRA simulation were post-processed to generate synthetic x-ray images for corroboration with the FXI images. An array of straight rays, each corresponding to an FXI pixel, was traced through the HYDRA mesh. The radiation transport equation was then integrated along each ray, using the resultant n_e, T_e, and LTE opacities. The result was convolved with the filter function of the 25 μm Be filter.

Emission from the polyimide skin was much brighter in the synthetic images than in the experimental images. We believe this is an artifact due to the LTE opacities used in the simulations, so the skin emission was removed from the images. The grayscale and background of the synthetic images were adjusted to qualitatively match the experimental images.

III.C. Synthetic SRS spectra

The simulation results were also post-processed for comparison to the time-resolved SRS spectra. At 10 ps intervals, a single ray was traced along the laser axis, 60 μm from the simulation axis. The resulting profiles of n_e, T_e, and plasma composition were input into NEWLIP, a package developed by E. A. Williams for performing kinetic laser-plasma interaction calculations[6]. The laser intensity was estimated from the input intensity by accounting for inverse bremsstrahlung absorption and defocusing. This agreed well with the zonal laser intensity output by HYDRA, but was less spatially noisy. At each time, the SRS gain coefficient was integrated along the ray as a function of scattered wavelength, giving the time-resolved gain spectrum.

IV. RESULTS AND ANALYSIS

IV.A. Laser propagation and hydrodynamics

Interpreting the Helen experiments requires understanding the hydrodynamics of gasbags. The laser beam rapidly deposits energy into the bag skin, causing it to ionize and explode outward. When the skin plasma falls below the critical density, the beam begins to propagate across the bag as a supersonic bleaching (ionization) wave, creating a long, constant-density interaction plateau.

The density profiles from one simulation are shown in Fig. 2. The localized energy deposition at the skin generates blast waves at the front and (later) back sides of the bag. The two blast waves propagate towards the center of the bag, shrinking the plateau. Similarly, the rapid heating and expansion in the laser channel drives a subsonic heat front (thermal hydro wave) radially outward. The radial flow behind the wave blows out the center of the channel, decreasing the electron density of the plateau. This effect is most evident at high densities,

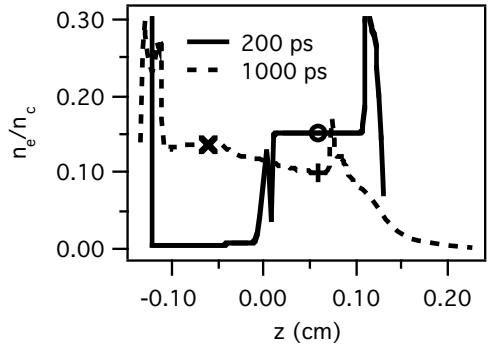

Fig. 2 Lineouts of simulated electron density at two times for Helen shot 2305 ($n_e = 0.15\ n_c$).

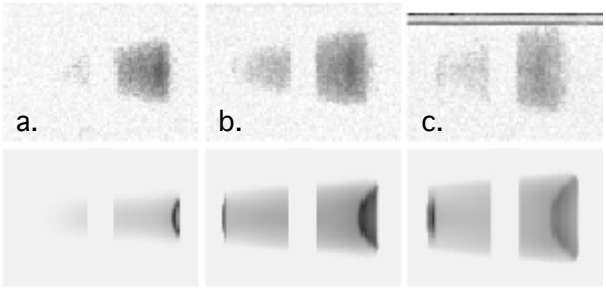

Fig. 3. Experimental (top row) and synthetic FXI images for shot 1811, at (a.) 360 ps, (b.) 860 ps, and (c.) 1250 ps from the start of the laser pulse. The laser travels from right to left.

where the laser is strongly absorbed.

Figure 3 shows experimental and synthetic FXI images from shot 1811, a gasbag with initial fill density $n_e = 0.16\ n_c$. The radial hydro wave defines the extent of the FXI images. The wave is formed first at the laser entrance side, forming a cone pointing from right to left. The extent of propagation and the shapes of the synthetic images agree well with the experiments. The success of HYDRA in modeling the experiments strongly suggests straightforward propagation across the bag.

IV.B. Raman backscatter

The total SRS backscatter for each shot is plotted against initial electron density in Fig. 4. As the initial density in the pure pentane bags increases, the SRS increases, peaking at 30 % near $n_e \approx 0.08\ n_c$. As density increases further, the total backscatter drops. The increase in backscatter with density is easily explained, as the SRS gain coefficient increases with density. The subsequent decrease beyond 0.08 n_c is more difficult to understand. One possible explanation is that the beam strongly filaments above $n_e \approx 0.1\ n_c$. The subsequent backscatter would then spread beyond the f/3 collection cone of the optics, resulting in an artificial drop in calorimeter signal.

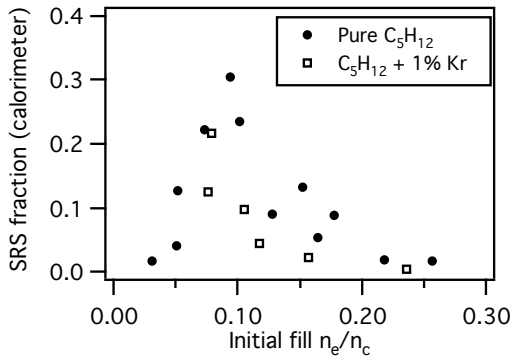

Fig. 4. Total SRS backscatter (fraction of input laser energy) as a function of initial bag density. Kr-doped bags have lower SRS, but show the same trend.

The NBI images, shown in Fig. 5, address this possibility. The spread of the backscatter actually decreases with increasing density. The low signal at higher density is consistent with lower total backscatter, not with backscatter outside of the beam cone.

The SRS gain spectra generated by post-processing the HYDRA simulations further suggest that filamentation plays a minor role in explaining the backscatter data. The experimental SRS streak spectra are shown in the top row of Fig. 6. At low density (< 0.1 n_c), the spectra are both straight and narrow. As density increases, the spectra broaden and tilt towards the laser wavelength of 527 nm. The synthetic spectra, shown in the bottom row of Fig. 6, closely follow the data. The experimental data do appear at slightly lower wavelength than the synthetic spectra, suggesting some "digging" in high-intensity speckles, physics not modeled in HYDRA; however, the tilt and spread of the experimental spectra are reproduced solely from bulk hydrodynamics and laser ray-tracing.

The role of hydrodynamics is more clearly seen by comparing Figs. 2 and 6. The three markers on Fig. 2 identify (n_e, T_e) pairs that correspond to the times and backscattered wavelengths on the synthetic spectrum for Fig. 6(e.). At early time, the bleaching wave is only halfway across the channel. The density plateau is short and flat, so the gain spectrum is narrow. At late time, the right side of the channel has blown-out to low density, corresponding to a wavelength closer to the laser wavelength. Backscatter from the left side, near the initial density, is near the initial wavelength. Axial gradients along one ray can explain the tilt and spread of the spectrum almost entirely.

Axial density gradients may also explain the drop in total SRS seen at high density in Fig. 4. Lower density bags absorb less strongly and have weaker radial hydro waves, so the plateaus remain flat. At higher density, axial density gradients may result in shorter resonant lengths along which SRS waves can grow. The higher absorption also results in lower intensity along the channel, further lowering the SRS gain. Further analysis is needed to determine the extent of the detuning.

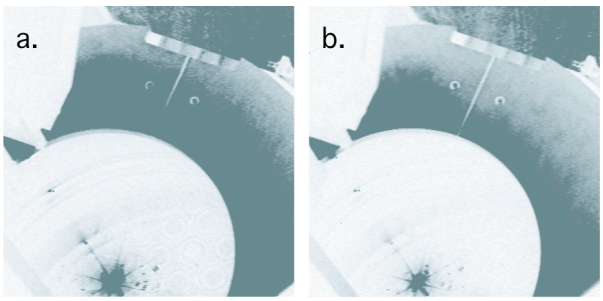

Fig. 5. Near-backscatter images from shots (a.) 2304 (initial $n_e \approx 0.10\ n_c$) and (b). 2305 (initial $n_e \approx 0.15\ n_c$). Dark indicates higher signal.

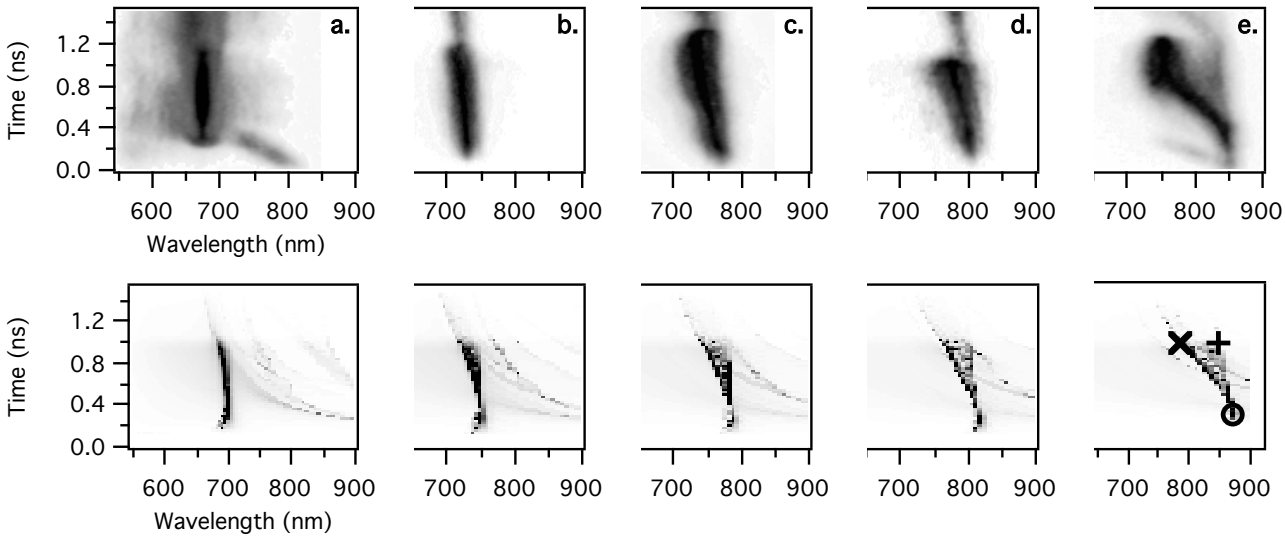

Fig. 6. Experimental (top) and synthetic SRS streak spectra. Markers correspond to Fig. 2. (a.) Shot 2303, 0.05 n_c. (b.) Shot 1809, 0.08 n_c. (c.) Shot 2304, 0.1 n_c. (d.) Shot 1813, 0.12 n_c. (e.) Shot 2305, 0.15 n_c.

V. CONCLUSIONS

Radiation-hydrodynamics simulations in HYDRA have been successfully applied to the analysis of 2 laser propagation and Raman backscatter experiments performed on the Helen laser. Experimental and simulated FXI images imply that the beam propagates across the gasbags in a straightforward way: Propagation can be explained by classical laser absorption and the resulting hydrodynamics, without invoking filamentation.

Synthetic SRS spectra accurately reproduce the tilt and spread of the experimental SRS streak spectra. The streak spectra also seem to be explained by straightforward laser propagation and hydrodynamics. Most features of the spectra can be explained solely by axial gradients along one ray. Axial density gradients may also explain the trend in total SRS with gasbag density. NBI images rule out severe beam spray as the cause of the decrease in total SRS backscatter with initial gasbag density.

ACKNOWLEDGMENTS

This work was performed under the auspices of the U.S. Department of Energy by the University of California Lawrence Livermore National Laboratory under contract No. W-7405-ENG-48. The author gratefully acknowledges valuable assistance from S. H. Glenzer, E. A. Williams, M. M. Marinak, and the Helen laser operations team.

REFERENCES

1. R. J. WALLACE, personal communication.
2. T. H. BETT, C. N. DANSON, P. JINKS, D. A. PEPLER, I. N. ROSS, AND R. M. STEVENSON, “Binary phase zone-plate arrays for laser-beam spatial-intensity distribution conversion,” *Applied Optics* **34**, 4025 (1995).
3. J. D. MOODY, B. J. MACGOWAN, R. L. BERGER, K. G. ESTABROOK, S. H. GLENZER, R. K. KIRKWOOD, W. L. KRUER, G. E. STONE, AND D. S. MONTGOMERY, “Experimental Study of Laser Beam Transmission and Power Accounting in a Large Scale Length Laser Plasma,” *Phys. Plasmas* 7, 3388 (2000), and references therein.
4. M. M. MARINAK, G. D. KERBEL, N. A. GENTILE, O. JONES, D. MUNRO, S. POLLAINE, T. R. DITTRICH, AND S. W. HAAN, “Three-dimensional HYDRA simulations of National Ignition Facility targets,” *Phys. Plasmas* **8**, 2275 (2001).
5. R. M. MORE, K. H. WARREN, D. A. YOUNG, AND G. B. ZIMMERMAN, “A New Quotidian Equation of State (QEOS) for Hot Dense Matter,” *Phys. Fluids* **31**, 3059 (1988).
6. E. A. WILLIAMS, “‘Platform-Independent’ Laser-Plasma Interaction Postprocessor for LASNEX,” in *1998 ICF Annual Report*, UCRL-LR-105820-98, 13 (1998).